

■ SUPPORTING INFORMATION

Sample preparation MLCC The capacitor was embedded into an epoxy resin (bisphenol A diglycidyl ether), cleaved transversally at the electrode end connections with a diamond saw, and polished mechanically with SiC paper (P1200 to P4000) and colloidal silica suspension (0.04 μm grain size). The Ni layer interspacing (Figure S-1) is determined by the capacitance, number of electrodes and electrode area set forth by the manufacturer.

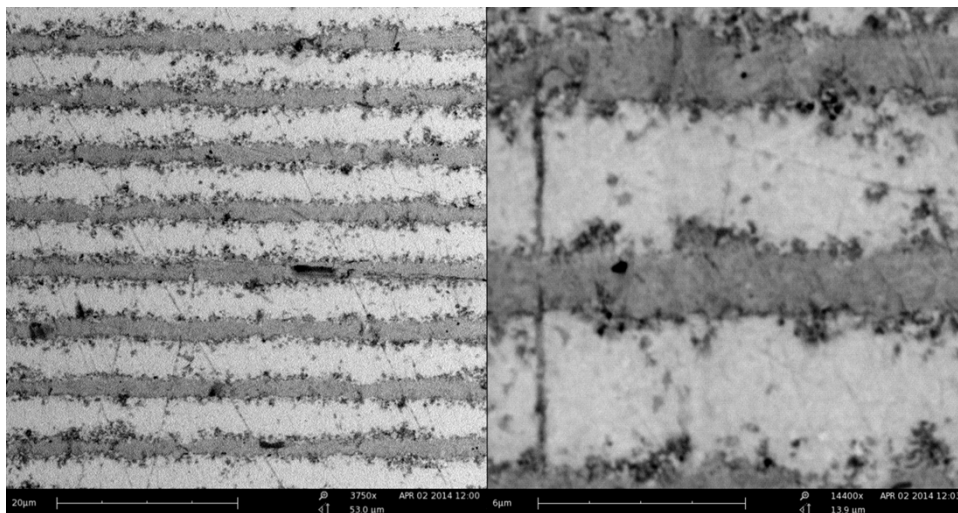


Figure S-1 Scanning electron microscopy images (5kV accelerating voltage, BSE, Phenom, Phenom-World, Eindhoven, Netherlands) of the polished MLCC surface.

Computational fluid dynamics simulation The ablation cell and connecting transfer tubing were modeled in AutoCAD™ (Autodesk™), imported into CFX (ANSYS™), and meshed with a fine grid of >1500 tetrahedrons mm^{-2} . Flow rates above *ca.* 1.7 l min^{-1} He push the Reynolds number R_e of this phase above 2000, out of the laminar flow regime and into the transitional zone ($1700 \leq R_e \leq 2300$) as the velocity gradient between the wall and center flow becomes too large, inducing turbulence and the potential formation of vortices.¹⁻³ As the gas flow rate is set near these levels, a statistical turbulence model, based on Reynolds Averaged Navier-Stokes (RANS) equations closed by Eddy Viscosity turbulence models (realizable $k-\epsilon$, $k-\omega$), was adopted. The bulk mass introduction rate at the He inlet was set to 4.516 mg s^{-1} (1.650 l min^{-1} , 293.15 K). The outlet was set to atmospheric pressure. He atoms reach an average velocity of $\sim 20.3 \text{ m s}^{-1}$ in the center of the central chamber (Figure S-1). The occurrence of turbulence in He is much less likely than in Ar or mixtures of these gases, as the inertia of He is lower compared to that of Ar (speed of sound in Ar >3 times lower than in He).

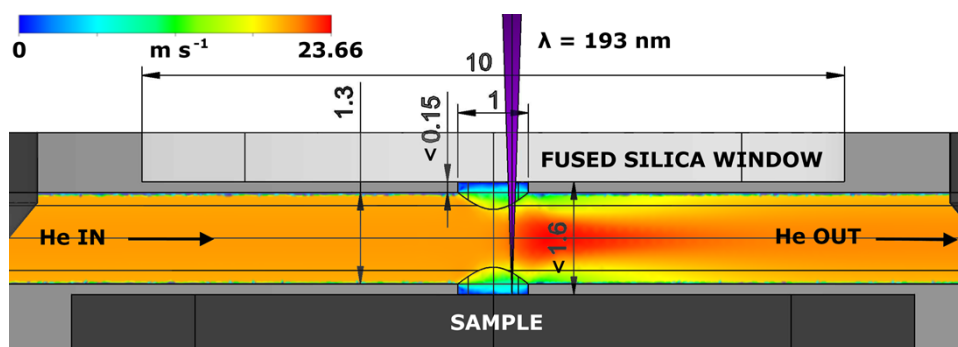


Figure S-2. Velocity vector scale distribution of He atoms within the cell.

Lateral resolution The MLCC can be considered as a square-wave grating with an object contrast ~ 1 , hence, an estimate of the lateral resolution can be computed. The dip-to-noise ratio resolution criterion by Senoner *et al.*⁴ was adapted for sequences of n peaks:

$$D_{avg} / \sigma_{NR} = \frac{\sum_n I_{max}/n - \sum_{n-1} I_{min}/(n-1)}{(4/S_{pp})^{1/2} \sigma_N} \geq 4$$

With D_{avg} the average dip, I_{max} and I_{min} , the median of 5 integrated peak areas centered around the maximum of the peak, and the minimum in between peaks, respectively, σ_{NR} the standard deviation of the reduced noise (noise ratio σ_N calculated for the electrode end connection region) and S_{pp} the number of sampling points per period of the grating. Figure S-3a displays a selected sequence of 8 peaks, a general linear combination of 8 Gaussians (LCG), fitted to the curve *via* the Levenberg–Marquardt algorithm, and a square wave corresponding to the MLCC pattern. The computation of the dip-to-noise ratio as a function of the interspace in between the layers (Figure S-3b) was based on simulating the response for a varying interspacing of the square-wave grating by virtually stacking resolved peak profiles as shown in Figure S-3c. The original dip-to-noise ratio of 28.2 was interpolated towards the limit of resolution in accordance to the criterion, and was estimated to be $0.3 \pm 0.1 \mu m$. This lateral resolution exceeds the virtual lateral resolution of $0.1 \mu m$, and is concurrent with the estimate for the limit of resolution for the LCG as defined by the Rayleigh criterion⁴. Considering the coarse transition between the electrodes and BaTiO₃ layers, the *effective* limit of resolution is expected to be better than the limit of resolution calculated.

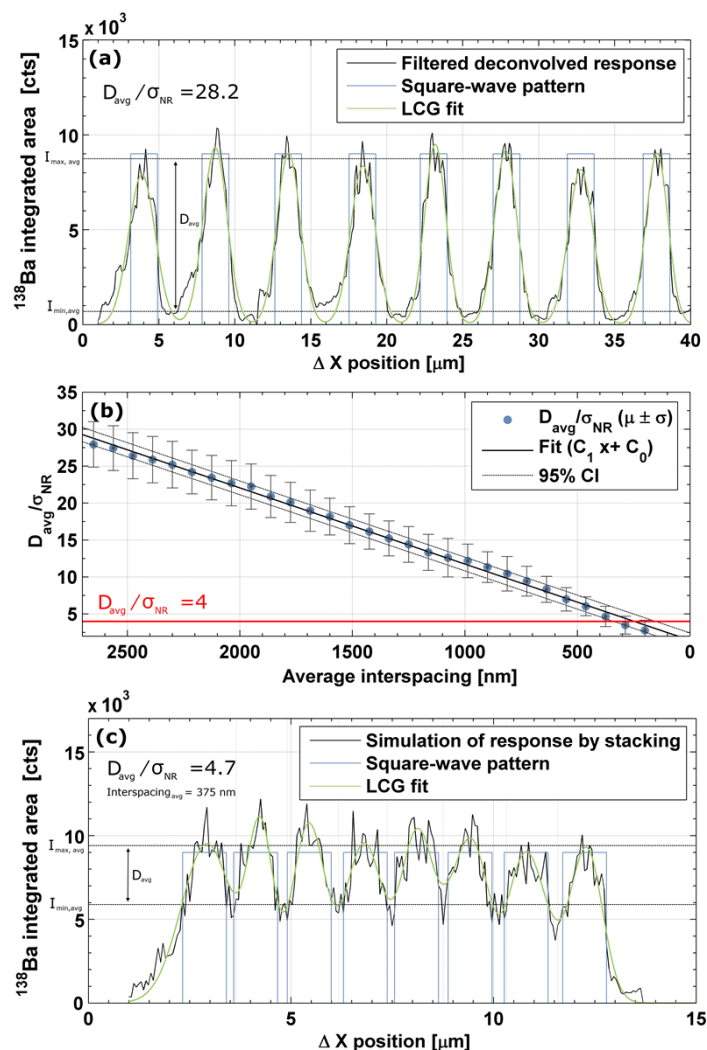


Figure S-3 (a) Detailed spatiotemporal change of the filtered deconvolved integrated peak areas in a selected sequence of 8 peaks ([204 μm, 244 μm] of the MLCC scan). (b) Dip-to-noise ratio as a function of the interspace in between the layers. (c)

Simulation of the response for a closely spaced layered MLCC structure, based on stacking the response of resolved layers in (a).

■ REFERENCES

1. D. Asogan, B. L. Sharp, C. J. P. O'Connor, D. A. Green and J. Wilkins, *J Anal Atom Spectrom*, 2011, **26**, 631.
2. H. Lindner, D. Autrique, J. Pisonero, D. Gunther and A. Bogaerts, *J Anal Atom Spectrom*, 2010, **25**, 295-304.
3. D. Bleiner and A. Bogaerts, *Spectrochimica Acta Part B: Atomic Spectroscopy*, 2007, **62**, 155-168.
4. M. Senoner, T. Wirth and W. E. S. Unger, *J Anal Atom Spectrom*, 2010, **25**, 1440.